Available online at www.sciencedirect.com
SCIENCE DIRECT®
Journal of Magnetic Resonance 175 (2005) 193–200
JMR Journal of Magnetic Resonance
www.elsevier.com/locate/jmr

Optimization of the irradiation power in chemical exchange dependent saturation transfer experiments

Phillip Zhe Sun *, Peter C.M. van Zijl, Jinyuan Zhou *

Division of MRI Research, Department of Radiology, Johns Hopkins University School of Medicine, Baltimore, MD 21205, USA
F.M. Kirby Research Center for Functional Brain Imaging, Kennedy Krieger Institute, Baltimore, MD 21205, USA

Received 12 February 2005; revised 6 April 2005
Available online 11 May 2005

Abstract

In chemical exchange dependent saturation transfer imaging experiments, exchangeable solute protons are saturated and the transfer of saturation to water is subsequently detected. When the applied irradiation power is comparable to the resonance frequency difference between the water protons and saturated solute protons, the proton transfer (PT) efficiency is reduced due to concomitant direct saturation effects. In this study, the PT process is modeled using a two-pool system. An empirical general proton transfer ratio (PTR) equation for arbitrary RF irradiation power is derived, and its optimal power to maximize the PTR is analyzed. The results are confirmed experimentally on 4.7 T using a poly-L-lysine solution. The theory provides a useful tool for optimizing the irradiation power of the PT sequences in the presence of direct saturation effects.

Keywords: Chemical exchange; CEST; APT; MT; Direct saturation; Spillover effect

1 Introduction

Although the study of chemical exchange processes by NMR is one of the oldest NMR topics [1–6], it has recently become of interest for several types of imaging experiments. Based on the concept originally proposed by Forsen and Hoffman [3] and using small molecules in solution, Balaban et al. [7–9] demonstrated that the proton transfer (PT) process between labile protons of solutes and water protons provides a detection sensitivity enhancement mechanism, an approach dubbed chemical exchange dependent saturation transfer (CEST). The solute content and exchange-related properties can thus be imaged indirectly and at higher sensitivity through the detection of the water signal. This mechanism is also being proposed for the use in designing new MRI contrast agents [10–13], which has tremendous applications in molecular and cellular imaging. Recently, it was shown [14,15] that endogenous mobile proteins and peptides in biological tissue could also be detected in this way. In the amide proton transfer (APT) imaging approach, the endogenous composite amide resonance around 8.3 ppm is saturated and detected indirectly to image tissue pH [14] or protein and peptide content [15].

The simplest experimental scheme for the investigation of proton exchange processes is to apply continuous low-power radiofrequency (RF) saturation (ω_1) on the exchangeable solute protons and subsequently monitor the transfer of saturation to water protons. If the applied RF field strength (in Hz) is negligible compared to the frequency difference ($\Delta\omega$) between the solute resonance and water peak, the PT efficiency improves with power and reaches a maximum, making optimization of the RF irradiation power straightforward. The weak saturation pulse assumption applies well to some

* Corresponding authors. Fax: +1 410 614 1948.
E-mail addresses: pzhesun@mri.jhu.edu (P.Z. Sun), jzhou@mri.jhu.edu (J. Zhou).

1090-7807/$ - see front matter © 2005 Elsevier Inc. All rights reserved.
doi:10.1016/j.jmr.2005.04.005

paramagnetic CEST (PARACEST) agents [11–13] and at high-magnetic fields used for high-resolution NMR studies (e.g., 11.7 T) but only approximately at field strengths commonly used for in vivo applications (1.5–4.7 T). For the case of irradiation pulses at intermediate strength or higher, the applied RF field can be comparable to the frequency difference between the solute resonance and water peak. In addition to saturation transfer effects, there are concomitant direct saturation effects on water protons (spillover effects [16–18]). As the RF power increases, the saturation transfer efficiency reaches its maximum while the spillover effects continue to increase. Thus, there is an optimal RF irradiation power at which the measured PT ratio (PTR) is maximized when both saturation transfer and spillover effects are considered.

The Bloch equations extended with exchange terms between the solute and water protons are commonly used to describe PT experiments. Even though a general solution for a broad range of RF irradiation power is complicated (see a comprehensive solution in the presence of the effects of off-resonance saturation, cross-relaxation, and chemical exchange published by Kingsley and Monahan [19,20]), concise results can be derived under certain assumptions. For example, based on the complete saturation of irradiated solute protons, the problem can be solved readily [3]. However, complete saturation can be obtained only under a very strong RF field; moreover, the spillover effects and ω_1 term are excluded in the expression. Thus, the solution is not applicable to our studies. Baguet and Roby [18,21] solved the Bloch equations for a two-pool system using the so-called double base transformation approach. For the strong saturation pulse case, the problem is simplified because all magnetization components perpendicular to corresponding effective fields are negligible. The double base transformation provides an effective way for studying the spillover effects. In this paper, the solution of the strong saturation pulse approximation is combined with that of the weak saturation pulse case, as used in several previous papers [11–13,22], and a reasonable approximation of an analytical solution is obtained for the full range of irradiation RF powers. Finally, the RF power at which PTR is maximal is derived and analyzed.

2 Theory

2.1 General Bloch equations for two-site exchange

We consider a two-pool proton exchange model that consists of a small pool for water-exchangeable solute protons (S) and a large pool for bulk water protons (W). Without loss of generality, it is assumed that the RF field is applied along the x-axis. The Bloch equations extended with exchange terms are then:

$$\frac{dM_X^W}{dt} = -R_{2W}M_X^W - \Delta\omega_W M_Y^W + k_{SW}M_X^S - k_{WS}M_X^W, \quad (1)$$

$$\frac{dM_Y^W}{dt} = \Delta\omega_W M_X^W - R_{2W}M_Y^W + k_{SW}M_Y^S - k_{WS}M_Y^W + \omega_1 M_Z^W, \quad (2)$$

$$\frac{dM_Z^W}{dt} = -\omega_1 M_Y^W - R_{1W}M_Z^W + k_{SW}M_Z^S - k_{WS}M_Z^W + R_{1W}M_0^W, \quad (3)$$

$$\frac{dM_X^S}{dt} = -R_{2S}M_X^S - \Delta\omega_S M_Y^S + k_{WS}M_X^W - k_{SW}M_X^S, \quad (4)$$

$$\frac{dM_Y^S}{dt} = \Delta\omega_S M_X^S - R_{2S}M_Y^S + k_{WS}M_Y^W - k_{SW}M_Y^S + \omega_1 M_Z^S, \quad (5)$$

$$\frac{dM_Z^S}{dt} = -\omega_1 M_Y^S - R_{1S}M_Z^S + k_{WS}M_Z^W - k_{SW}M_Z^S + R_{1S}M_0^S, \quad (6)$$

where $M_{X,Y,Z}^{W,S}$ are the X, Y, and Z components of the magnetizations; $M_0^{W,S}$ are the equilibrium magnetizations; $R_{1W,S}$ and $R_{2W,S}$ are the longitudinal and transverse relaxation rates, respectively; k_{SW} and k_{WS} are the exchange rates of protons from pool S to pool W and vice versa. When the spin system is at equilibrium, the detailed balance relationship holds: $k_{SW}M_0^S = k_{WS}M_0^W$. In contrast with conventional magnetization transfer (MT) experiments [23,24], in which the two relevant pools (solid-like macromolecules and bulk water) can be treated as having identical chemical shift and are distinguished only by relaxation parameters, the present system consists of two proton pools with different chemical shifts, $\delta\omega_W$ and $\delta\omega_S$, and different relaxation parameters. In addition, the transverse magnetization-related exchange terms have been included in the equations here, whereas they have often been omitted for the description of conventional MT [25,26] despite a previous report [27] of possible contributions.

Magnetization transfer effects are usually assessed using the so-called z-spectrum [28], in which the water signal intensity is plotted as a function of saturation offset. Because direct water saturation effects are symmetric with respect to the water resonance frequency, the spillover effects can be removed partially by a z-spectrum asymmetry analysis [8,9]. In this analysis, the PTR is defined as the difference of water signal intensities when the irradiation pulses are applied at the exchangeable solute proton frequency (M_{sat}^W) and at a reference frequency symmetrically at the opposite side of the water resonance (M_{ref}^W), normalized by the measurement without any saturation pulses (M_0^W):

$$PTR = \frac{M_{ref}^W - M_{sat}^W}{M_0^W}. \quad (7)$$

2.2 Strong saturation pulse case

Based on the notation used by Baguet and Roby [18,21], the coupled Bloch equations for the two-pool model in the new coordinates (X', Y', Z') can be written as:

$$\frac{\mathrm{d}}{\mathrm{d}t}\begin{pmatrix} M^{\mathrm{W}}_{X'} \\ M^{\mathrm{W}}_{Y'} \\ M^{\mathrm{W}}_{Z'} \\ M^{\mathrm{S}}_{X'} \\ M^{\mathrm{S}}_{Y'} \\ M^{\mathrm{S}}_{Z'} \end{pmatrix} = \begin{pmatrix} S_{\mathrm{W}} & T_{\mathrm{S}} \\ T_{\mathrm{W}} & S_{\mathrm{S}} \end{pmatrix} \times \begin{pmatrix} M^{\mathrm{W}}_{X'} \\ M^{\mathrm{W}}_{Y'} \\ M^{\mathrm{W}}_{Z'} \\ M^{\mathrm{S}}_{X'} \\ M^{\mathrm{S}}_{Y'} \\ M^{\mathrm{S}}_{Z'} \end{pmatrix} + \begin{pmatrix} R_{1\mathrm{W}} M^{\mathrm{W}}_0 \sin\theta_{\mathrm{W}} \\ 0 \\ R_{1\mathrm{W}} M^{\mathrm{W}}_0 \cos\theta_{\mathrm{W}} \\ R_{1\mathrm{S}} M^{\mathrm{S}}_0 \sin\theta_{\mathrm{S}} \\ 0 \\ R_{1\mathrm{S}} M^{\mathrm{S}}_0 \cos\theta_{\mathrm{S}} \end{pmatrix}, \tag{8}$$

where the matrix elements are defined as:

$$S_{\mathrm{W}} = \begin{pmatrix} -(r_{1\mathrm{W}}\sin^2\theta_{\mathrm{W}} + r_{2\mathrm{W}}\cos^2\theta_{\mathrm{W}}) & -\sqrt{\omega_1^2 + \Delta\omega_{\mathrm{W}}^2} & -\sin\theta_{\mathrm{W}}\cos\theta_{\mathrm{W}}(r_{1\mathrm{W}} - r_{2\mathrm{W}}) \\ \sqrt{\omega_1^2 + \Delta\omega_{\mathrm{W}}^2} & -r_{2\mathrm{W}} & 0 \\ -\sin\theta_{\mathrm{W}}\cos\theta_{\mathrm{W}}(r_{1\mathrm{W}} - r_{2\mathrm{W}}) & 0 & -(r_{2\mathrm{W}}\sin^2\theta_{\mathrm{W}} + r_{1\mathrm{W}}\cos^2\theta_{\mathrm{W}}) \end{pmatrix}, \tag{9}$$

$$T_{\mathrm{W}} = k_{\mathrm{WS}} \begin{pmatrix} \cos(\theta_{\mathrm{W}} - \theta_{\mathrm{S}}) & 0 & -\sin(\theta_{\mathrm{W}} - \theta_{\mathrm{S}}) \\ 0 & 1 & 0 \\ \sin(\theta_{\mathrm{W}} - \theta_{\mathrm{S}}) & 0 & \cos(\theta_{\mathrm{W}} - \theta_{\mathrm{S}}) \end{pmatrix}, \tag{10}$$

and similarly for S_{S} and T_{S}. In these equations, $\theta_{\mathrm{W,S}} = \tan^{-1}(\frac{\omega_1}{\Delta\omega_{\mathrm{W,S}}})$, $r_{1\mathrm{W}} = R_{1\mathrm{W}} + k_{\mathrm{WS}}$, $r_{1\mathrm{S}} = R_{1\mathrm{S}} + k_{\mathrm{SW}}$, $r_{2\mathrm{W}} = R_{2\mathrm{W}} + k_{\mathrm{WS}}$, and $r_{2\mathrm{S}} = R_{2\mathrm{S}} + k_{\mathrm{SW}}$.

When the power of the applied saturation pulse (in Hz) is much stronger than the relaxation and exchange rates, all of the magnetizations perpendicular to the corresponding effective fields can be approximated to be zero. Thus, Eq. (8) can be simplified to two equations describing the magnetization components along their corresponding effective field orientations. This greatly reduces the complexity of the problem, and the steady-state analytical solution for the water magnetization can be shown to be:

$$M^{\mathrm{W}}_{Z'} = \frac{R_{1\mathrm{W}}R_{Z\mathrm{S}}\cos\theta_{\mathrm{W}} + R_{1\mathrm{S}}k_{\mathrm{WS}}\cos\theta_{\mathrm{S}}\cos(\theta_{\mathrm{W}} - \theta_{\mathrm{S}})}{R_{Z\mathrm{W}}R_{Z\mathrm{S}} - k_{\mathrm{WS}}k_{\mathrm{SW}}\cos^2(\theta_{\mathrm{W}} - \theta_{\mathrm{S}})} M^{\mathrm{W}}_0, \tag{11}$$

where $R_{Z\mathrm{W,S}} = r_{1\mathrm{W,S}}\cos^2\theta_{\mathrm{W,S}} + r_{2\mathrm{W,S}}\sin^2\theta_{\mathrm{W,S}}$. When the saturation pulse is followed by a crusher gradient, an excitation pulse, and finally an acquisition period, the measured signal is the magnitude of the magnetization along the Z-axis:

$$M^{\mathrm{W}}_Z = \cos\theta_{\mathrm{W}} \times \frac{R_{1\mathrm{W}}R_{Z\mathrm{S}}\cos\theta_{\mathrm{W}} + R_{1\mathrm{S}}k_{\mathrm{WS}}\cos\theta_{\mathrm{S}}\cos(\theta_{\mathrm{W}} - \theta_{\mathrm{S}})}{R_{Z\mathrm{W}}R_{Z\mathrm{S}} - k_{\mathrm{WS}}k_{\mathrm{SW}}\cos^2(\theta_{\mathrm{W}} - \theta_{\mathrm{S}})} M^{\mathrm{W}}_0. \tag{12}$$

If the irradiation pulses are applied on resonance on the solute protons, $\theta^{\mathrm{sat}}_{\mathrm{S}} = \frac{\pi}{2}$ and $\theta^{\mathrm{sat}}_{\mathrm{W}} = \tan^{-1}(\frac{\omega_1}{\Delta\omega}) = \theta$. Thus, the water magnetization can be simplified to be:

$$M^{\mathrm{W}}_{\mathrm{sat}} = \frac{R_{1\mathrm{W}}r_{2\mathrm{S}}\cos^2\theta}{r_{Z\mathrm{W}}r_{2\mathrm{S}} - k_{\mathrm{WS}}k_{\mathrm{SW}}\sin^2\theta} M^{\mathrm{W}}_0, \tag{13}$$

in which $r_{Z\mathrm{W}} = r_{1\mathrm{W}}\cos^2\theta + r_{2\mathrm{W}}\sin^2\theta$. For the reference scan, the effective fields for the water and solute protons are rotated by tilting angles $\theta^{\mathrm{ref}}_{\mathrm{W}} = \tan^{-1}(\frac{-\omega_1}{\Delta\omega}) = -\theta$ and $\theta^{\mathrm{ref}}_{\mathrm{S}} = \tan^{-1}(\frac{-\omega_1}{2\Delta\omega}) \approx -\theta/2$, respectively. The approximation in the expression of $\theta^{\mathrm{ref}}_{\mathrm{S}}$ is readily met for the weak and intermediate irradiation pulse cases, in which the optimal power is usually much smaller than the chemical shift difference between the solute and water protons. As a consequence, the PTR obtained through the double base transformation approach is:

$$\mathrm{PTR}^{\mathrm{strong}} = \frac{R_{1\mathrm{W}}r_{Z\mathrm{S}}\cos^2\theta + R_{1\mathrm{S}}k_{\mathrm{WS}}\cos\theta\cos^2(\theta/2)}{r_{Z\mathrm{W}}r_{Z\mathrm{S}} - k_{\mathrm{WS}}k_{\mathrm{SW}}\cos^2(\theta/2)} - \frac{R_{1\mathrm{W}}r_{2\mathrm{S}}\cos^2\theta}{r_{Z\mathrm{W}}r_{2\mathrm{S}} - k_{\mathrm{WS}}k_{\mathrm{SW}}\sin^2\theta}, \tag{14}$$

in which $r_{Z\mathrm{S}} = r_{1\mathrm{S}}\cos^2(\theta/2) + r_{2\mathrm{S}}\sin^2(\theta/2)$.

2.3 Weak saturation pulse case

When the irradiation pulse is of very low power, the spillover effects are generally negligible. In this case, the set of six coupled Bloch equations for the two pools can be approximated by four equations for the Y and Z magnetization components:

$$\frac{\mathrm{d}M^{\mathrm{W}}_Y}{\mathrm{d}t} = -R_{2\mathrm{W}}M^{\mathrm{W}}_Y + k_{\mathrm{SW}}M^{\mathrm{S}}_Y - k_{\mathrm{WS}}M^{\mathrm{W}}_Y, \tag{15}$$

$$\frac{\mathrm{d}M^{\mathrm{W}}_Z}{\mathrm{d}t} = -R_{1\mathrm{W}}M^{\mathrm{W}}_Z + k_{\mathrm{SW}}M^{\mathrm{S}}_Z - k_{\mathrm{WS}}M^{\mathrm{W}}_Z + R_{1\mathrm{W}}M^{\mathrm{W}}_0, \tag{16}$$

$$\frac{\mathrm{d}M^{\mathrm{S}}_Y}{\mathrm{d}t} = -R_{2\mathrm{S}}M^{\mathrm{S}}_Y + k_{\mathrm{WS}}M^{\mathrm{W}}_Y - k_{\mathrm{SW}}M^{\mathrm{S}}_Y + \omega_1 M^{\mathrm{S}}_Z, \tag{17}$$

$$\frac{\mathrm{d}M^{\mathrm{S}}_Z}{\mathrm{d}t} = -\omega_1 M^{\mathrm{S}}_Y - R_{1\mathrm{S}}M^{\mathrm{S}}_Z + k_{\mathrm{WS}}M^{\mathrm{W}}_Z - k_{\mathrm{SW}}M^{\mathrm{S}}_Z + R_{1\mathrm{S}}M^{\mathrm{S}}_0. \tag{18}$$

When the duration of an irradiation pulse is long enough, both pools can reach a steady state. The magnetization for water protons along the z-axis is then [22]:

$$M^{\mathrm{W}}_{\mathrm{sat}} = \left(1 - \frac{k_{\mathrm{WS}}\alpha}{r_{1\mathrm{W}}}\right) M^{\mathrm{W}}_0, \tag{19}$$

where $\alpha = \frac{\omega_1^2}{pq + \omega_1^2}$, $p = r_{2\mathrm{S}} - \frac{k_{\mathrm{SW}}k_{\mathrm{WS}}}{r_{2W}}$, and $q = r_{1\mathrm{S}} - \frac{k_{\mathrm{SW}}k_{\mathrm{WS}}}{r_{1\mathrm{W}}}$. Because the spillover effects are assumed to be negligible

for weak RF pulses, the reference measurement in the asymmetry analysis is simply equal to its equilibrium magnetization M_0^{W}. The PTR for the weak saturation pulse case at steady state is therefore:

$$\mathrm{PTR}^{\mathrm{weak}} = \frac{k_{\mathrm{WS}}\alpha}{r_{1\mathrm{W}}}. \tag{20}$$

2.4 General RF saturation case

The solutions of the above two extreme cases are applicable only when the power of the irradiation pulses is within the range justifying the corresponding assumptions. The solution for the strong saturation pulse case starts from a maximal PTR value ($k_{\mathrm{WS}}/r_{1\mathrm{W}}$) at $\omega_1 = 0$ and decreases with increasing RF power. However, at weak RF power, the saturation transfer effects should be negligible and thus the PTR has to be minimal. This deviation is due to the inappropriate assumption of the complete saturation of magnetizations perpendicular to their corresponding effective fields regardless of the RF irradiation power, which is used to derive Eqs. (11)–(13). On the other hand, there are no spillover effects for the weak RF pulse case, and its solution can describe the PT process well. As the RF power increases, the solute pool experiences more saturation, and the PT efficiency increases from zero to a maximum. It is important to note that the solutions for these two extreme cases have the same maximal PTR. Thus, the product of these two solutions normalized by the maximal PTR is able to predict the correct PTR for the two extreme cases of weak and strong irradiation field:

$$\mathrm{PTR} = \alpha\left[\frac{R_{1\mathrm{W}}r_{\mathrm{ZS}}\cos^2\theta + R_{1\mathrm{S}}k_{\mathrm{WS}}\cos\theta\cos^2(\theta/2)}{r_{\mathrm{ZW}}r_{\mathrm{ZS}} - k_{\mathrm{WS}}k_{\mathrm{SW}}\cos^2(\theta/2)} - \frac{R_{1\mathrm{W}}r_{2\mathrm{S}}\cos^2\theta}{r_{\mathrm{ZW}}r_{2\mathrm{S}} - k_{\mathrm{WS}}k_{\mathrm{SW}}\sin^2\theta}\right], \tag{21}$$

which can be further demonstrated to provide an empirical analytical description for arbitrary RF pulses (see Fig. 2). It can be shown that PTR increases with RF pulse power initially because of the more effective magnetization saturation, and it decreases with further increase of the RF power when the spillover effects become significant. Thus, there is an optimal RF power at which the PTR is maximal under the influence of competing saturation transfer and direct saturation processes. By nulling the first order derivative of the unified solution with respect to ω_1, the optimal RF power can be obtained (see Appendix A):

$$\omega_1 = \Delta\omega\sqrt{A} = \sqrt{pq\left\{\sqrt{1 + \frac{4(f_{\mathrm{S}} + f_{\mathrm{W}})\bar{\beta}\eta_{2\mathrm{S}}}{\left[f_{\mathrm{S}}\eta_{2\mathrm{S}}(1 + 2\bar{\beta} + \eta_{\mathrm{S}} + 4\eta_{\mathrm{W}}) + f_{\mathrm{W}}(4 + 4\beta^2 + \eta_{2\mathrm{S}}(5 + \eta_{2\mathrm{S}} + 8\eta_{\mathrm{W}}) - 4\beta(2 + \eta_{2\mathrm{S}} + \eta_{2\mathrm{S}}\eta_{\mathrm{W}}))\right]}\frac{\Delta\omega^2}{pq}} - 1\right\}}, \tag{22}$$

where $\beta = \frac{k_{\mathrm{WS}}k_{\mathrm{SW}}}{r_{1\mathrm{W}}r_{1\mathrm{S}}}$, $\bar{\beta} = 1 - \beta$, $\eta_{\mathrm{W}} = \frac{r_{\mathrm{W}}}{r_{1\mathrm{W}}}$, $\eta_{\mathrm{S}} = \frac{r_{\mathrm{S}}}{r_{1\mathrm{S}}}$, $\eta_{2\mathrm{S}} = \frac{r_{2\mathrm{S}}}{r_{1\mathrm{S}}}$, $r_{\mathrm{W}} = r_{2\mathrm{W}} - r_{1\mathrm{W}}$, $r_{\mathrm{S}} = r_{2\mathrm{S}} - r_{1\mathrm{S}}$, $\eta_{2\mathrm{S}} = \frac{r_{2\mathrm{S}}}{r_{1\mathrm{S}}}$, $f_{\mathrm{W}} = \frac{R_{1\mathrm{W}}}{r_{1\mathrm{W}}}$, and $f_{\mathrm{S}} = \frac{R_{1\mathrm{S}}}{k_{\mathrm{SW}}}$.

3 Materials and methods

Experiments were carried out on a 4.7 T Bruker Biospec Imager at the room temperature of approximately 25 °C. Two hundred milligram poly-L-lysine (PLL, MW >300 kDa) containing a high concentration of exchangeable amide protons was purchased from Sigma–Aldrich (St. Louis, MO) and added to 20 ml PBS buffer. The pH was adjusted to 7.4. The solution was then transferred into an NMR tube of 20 mm ID and sealed with a plastic plug and cap. The NMR tube was positioned coaxially within a 70 mm ID volume coil. The MRI measurements utilized a long irradiation pulse followed by a single-shot echo planar imaging (EPI) readout. The duration of the continuous saturation pulse was 15 s with a repetition time (TR) of 30 s. All images had a field of view (FOV) of 32 mm × 32 mm and a matrix size of 64 × 64. The slice thickness was 5 mm. The power levels were varied from 0.125 to 6.25 μT.

Modeling and data processing were conducted using a self-written Matlab code on a Dell Precision 450 Desktop. The extended Bloch equations (Eqs. (1)–(6)) were solved using an ordinary differential equation (ODE) solver of Matlab and the scalar relative error tolerance for all simulated magnetization components was 10^{-6}. The irradiation pulse duration was set to be 15 s and the spins were assumed at the equilibrium state initially. The model parameters used were $T_{1\mathrm{W}} = 3$ s, $T_{2\mathrm{W}} = 2$ s, $T_{1\mathrm{S}} = 0.77$ s, $T_{2\mathrm{S}} = 33$ ms, $k_{\mathrm{SW}} = 200$ Hz, and $M_0^{\mathrm{W}}/M_0^{\mathrm{S}} = 2000$. The experimental PTR as a function of RF power was fitted according to Eq. (21). We used $T_{1\mathrm{W}} = 3$ s and $T_{2\mathrm{W}} = 2$ s, which were estimated based on the measurements from PBS buffer. We assumed $T_{1\mathrm{S}} = 0.77$ s and $T_{2\mathrm{S}} = 33$ ms [29], which have relatively small effects on PTR. The pool ratio was approximately 2300 for our PLL phantom. The only remaining unknown parameter is the exchange rate, k_{SW}, which can be obtained by fitting the experimental results using Eq. (21).

4 Results and discussion

Fig. 1 shows the z-spectra and corresponding MT asymmetry (or PT) spectra using numerical simulations

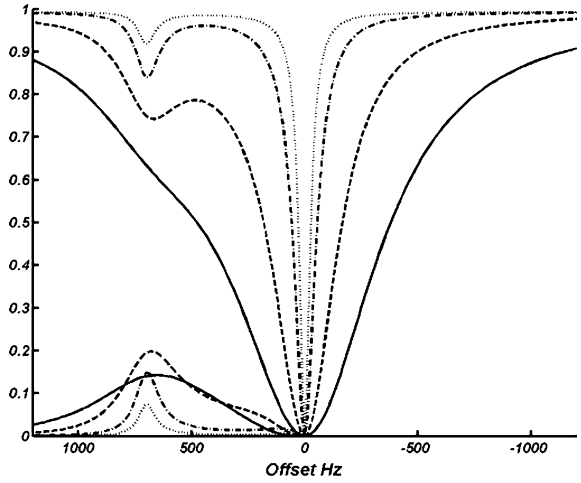

Fig. 1. Simulated z-spectra (middle) and MTR asymmetry spectra (bottom-left) at 4.7 T for several irradiation powers for a two-pool exchange model using a set of six coupled Bloch equations. The model parameters used are $T_{1W} = 3$ s, $T_{2W} = 2$ s, $T_{1S} = 0.77$ s, $T_{2S} = 33$ ms, $k_{SW} = 200$ Hz, and $M_0^W/M_0^S = 2000$. The dotted, dash-dotted, dashed, and solid lines correspond to the cases of irradiation pulse powers of 0.5, 1, 3, and 7 μT (1 μT = 42.6 Hz), respectively.

of the set of six coupled Bloch equations. When the irradiation power is low (~0.5 μT, 1 μT = 42.6 Hz), the saturation efficiency for the solute resonance is limited, and the water signal reduction is small. The PT efficiency increases gradually with the applied RF power (1–3 μT), as reflected by increased PTR at the exchangeable solute proton frequency. The PTR increases and reaches its maximal value at an optimal RF power. From this point on, any further power increase will introduce additional spillover effects, thus reducing PTR. Fig. 2A shows the theoretical plot of PTR as a function of irradiation power, in which the analytical solutions and numerical simulations are compared. The strong saturation pulse approximation and weak saturation pulse approximation, respectively, conform to the numerically simulated PTR curve based on the set of six coupled Bloch equations only when the RF power is within their assumptive regimes. Our theory well predicts the PTR across a wide range of irradiation powers and, for the chosen case, an optimal irradiation power of 2.49 μT to maximize the PTR. Fig. 2B shows the PTR plots calculated for several different exchange rates. Because faster PT processes can better compete with the spillover effects, the optimal RF power increases with exchange rates. It is important to note that the optimal irradiation power shows a negligible dependence on the pool ratio (despite changed PTR, see Fig. 2C) and the T_{2S} value (too close to show). When the pool ratio changes from 1500, 2000 to 3000 (k_{WS} changed according to the detailed balance equation), the optimal power changes from 2.42, 2.49 to 2.55 μT. When the T_{2S} varies from 20, 33 to 50 ms, the optimal power changes from 2.55, 2.49, and 2.45 μT.

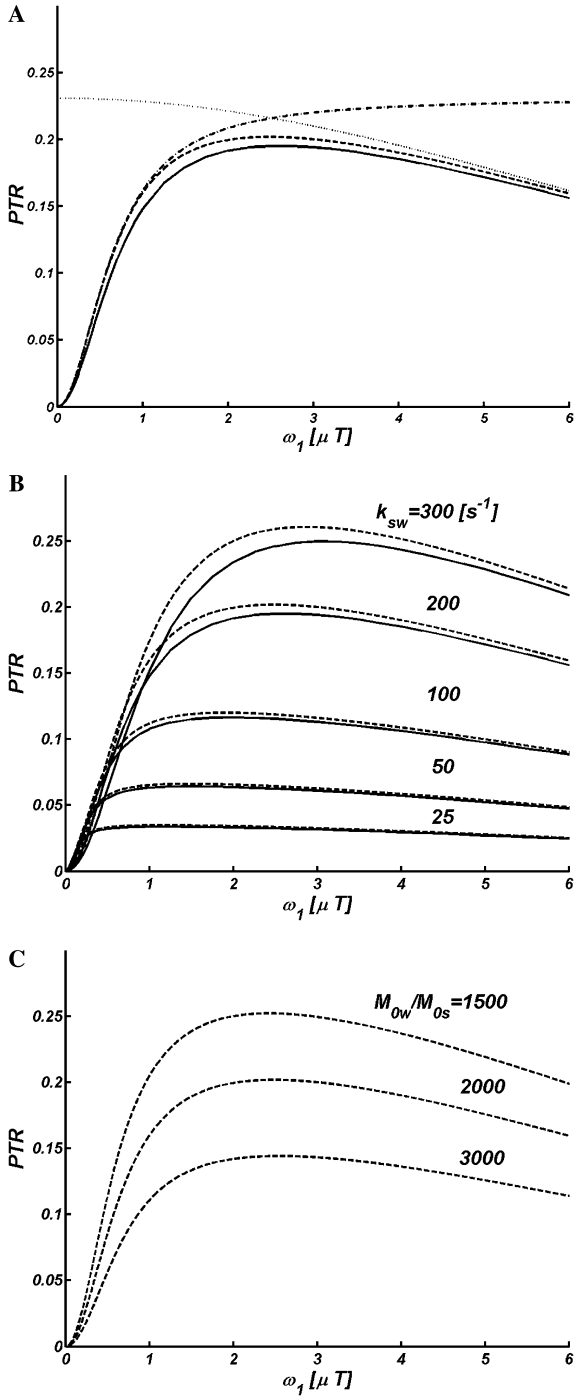

Fig. 2. Calculated PTR at 4.7 T from the two-pool Bloch equations as a function of RF irradiation power. Numerical results (solid) based on a set of six coupled Bloch equations and analytical solutions for the strong saturation pulse approximation (dotted), weak saturation pulse approximation (dash-dotted), and the empirical general case (dashed). (A) Comparison of the four different solutions. The model parameters are the same as used in Fig. 1. (B) Influence of the exchange rates on the PT efficiency. (C) Effect of the pool ratio on the optimal saturation power.

Fig. 3 shows the z-spectra and corresponding PT spectra acquired on the PLL solution at 4.7 T. In agreement with the theoretical results, the saturation transfer

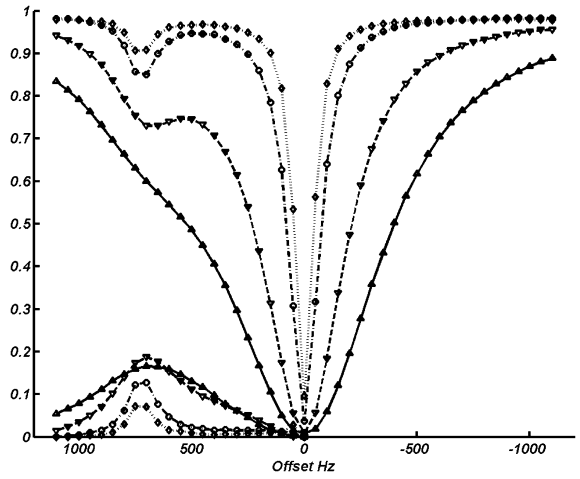

Fig. 3. Measured z-spectra (middle) and MTR asymmetry spectra (bottom-left) of a PLL phantom at 4.7 T (1%w/w, pH 7.4, 25 °C). TR was 30 s and the RF irradiation pulse duration was 15 s. The powers used were 0.5 μT (dotted), 1 μT (dash-dotted), 3 μT (dashed), and 6.25 μT (solid). At high-RF irradiation power, the peak of the asymmetry spectra decreases, indicating a lowered PTR.

effect increases initially with the power of irradiation pulses, but decreases at higher power levels. The plot of measured PTR as a function of irradiation power is shown in Fig. 4, showing an optimal saturation power of approximately 2.5 μT, which is close to 2.43 μT calculated by Eq. (22). The fitted exchange rate using Eq. (21) was 197 Hz, which is reasonable within experimental errors for our experimental conditions (25 °C and pH 7.4). These experimental data clearly indicate that the unified PTR formula can successfully simulate the PT process across the full range of RF irradiation powers and predict the existence of an optimal saturation power consequential to the competing effects of saturation transfer and spillover effects.

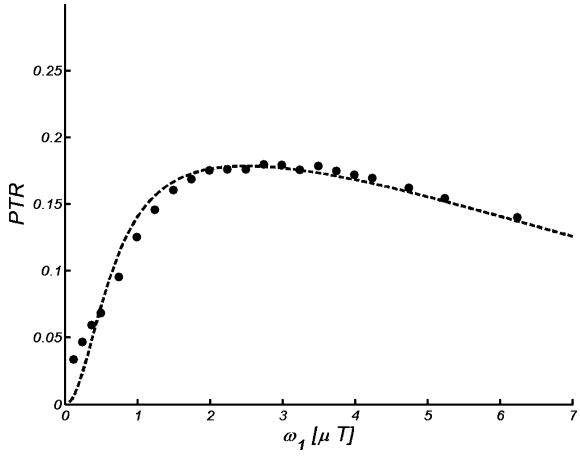

Fig. 4. Measured PTR (solid circle) for the PLL solution as a function of RF irradiation power. The dashed line is the fitted result using Eq. (21). The PTR increases and approaches a maximum at an irradiation power of 2.5 μT, which is close to 2.43 μT predicted by Eq. (22).

The RF power dependence for the PT process was modeled using the Bloch equations extended with exchange terms. An empirical PTR solution for arbitrary RF irradiation power and the optimal power to obtain the maximal PTR were derived for a two-pool system of the exchangeable solute protons and water protons. We should note that the Taylor expansion up to the second order of the effective tilting angles was used in our derivation of the optimal power (see Appendix A). Thus, the solution may not be accurate to predict the optimal power where the tilting angles are significant (e.g., small chemical shift difference between the exchangeable solute protons and water protons, low-magnetic field system, and/or very high-RF power). In addition, the increased spillover effects lead to a wider PT spectrum, in particular, when the irradiation power is beyond the optimal power level. If there are multiple pools of exchangeable solute protons in the system, such a long tail in the PT spectra may introduce an additional RF saturation power dependence to other solute protons. The Bloch equations for multiple pools are required to account for these effects.

5 Conclusions

In this study, an empirical analytical solution for assessing the PT process across a complete range of RF powers is derived by combing the analytical solutions for the strong and weak saturation pulse cases. In addition, an optimal RF power is derived for the maximal PT efficiency when both PT and direct saturation effects are present.

Acknowledgments

This study was supported in part by grants from NIH/NIBIB (EB02634), NIH/NIBIB (EB02666), and the Whitaker Foundation. We are grateful to Hardes Yong Xiao at Massachusetts Institute of Technology for useful conversations.

Appendix A

Because the optimal power is usually smaller than the chemical shift difference between the solute and water protons and the effective field is only slightly perturbed from the z-axis, we have the trigonometric expansions: $\cos^2\theta = 1 - \theta^2$ and $\sin^2\theta = \theta^2$. Using these approximations, r_{ZW} and r_{ZS} can be simplified as:

$$\begin{aligned} r_{ZW} &= r_{1W}\cos^2\theta + r_{2W}\sin^2\theta \\ &\approx r_{1W}(1-\theta^2) + r_{2W}\theta^2 = r_{1W} + A(r_{2W} - r_{1W}) \\ &= r_{1W} + Ar_W, \end{aligned} \tag{A.1}$$

$$r_{ZS} = r_{1S}\cos^2(\theta/2) + r_{2S}\sin^2(\theta/2) \approx r_{1S}\left(1-\frac{\theta^2}{4}\right) + r_{2S}\frac{\theta^2}{4}$$
$$= r_{1S} + \frac{A}{4}(r_{2S} - r_{1S}) = r_{1S} + \frac{A}{4}r_S, \quad (A.2)$$

where $A = \theta^2$, $r_W = r_{2W} - r_{1W}$, and $r_S = r_{2S} - r_{1S}$. Thus, one has:

$$\mathrm{PTR} = \alpha\left[\frac{R_{1W}\left(r_{1S}+\frac{4}{4}r_S\right)(1-A) + R_{1S}k_{WS}\left(1-\frac{4}{2}\right)\left(1-\frac{4}{4}\right)}{(r_{1W}+Ar_W)\left(r_{1S}+\frac{4}{4}r_S\right) - k_{WS}k_{SW}\left(1-\frac{4}{4}\right)} - \frac{R_{1W}r_{2S}(1-A)}{(r_{1W}+Ar_W)r_{2S} - k_{WS}k_{SW}A}\right]. \quad (A.3)$$

When neglecting the second-order terms of A, we obtain:

$$\mathrm{PTR} = \alpha\left[\frac{(f_W+\beta f_S) + \left(\frac{f_W\eta_S - 3\beta f_S - 4f_W}{4}\right)A}{(1-\beta) + \left(\frac{\eta_S+4\eta_W+\beta}{4}\right)A} + \frac{-f_W + f_W A}{1+\left(\eta_W - \frac{\beta}{\eta_{2S}}\right)A}\right]$$
$$= \alpha\left(\frac{B_1+B_2A}{B_3+B_4A} + \frac{C_1+C_2A}{C_3+C_4A}\right), \quad (A.4)$$

where $\beta = \frac{k_{WS}k_{SW}}{r_{1W}r_{1S}}$, $\eta_W = \frac{r_W}{r_{1W}}$, $\eta_S = \frac{r_S}{r_{1S}}$, $\eta_{2S} = \frac{r_{2S}}{r_{1S}}$, $f_W = \frac{R_{1W}}{r_{1W}}$, $f_S = \frac{R_{1S}}{k_{SW}}$, $B_1 = f_W + \beta f_S$, $B_2 = \frac{f_W\eta_S - 3\beta f_S - 4f_W}{4}$, $B_3 = 1-\beta$, $B_4 = \frac{\eta_S+4\eta_W+\beta}{4}$, $C_1 = -f_W$, $C_2 = f_W$, $C_3 = 1$, and $C_4 = \eta_W - \frac{\beta}{\eta_{2S}}$.

The unified PTR can be further expanded to be:

$$\mathrm{PTR} = \alpha\left\{\frac{B_1}{B_3}\left[1+\left(\frac{B_2}{B_1}-\frac{B_4}{B_3}\right)A\right] + \frac{C_1}{C_3}\left[1+\left(\frac{C_2}{C_1}-\frac{C_4}{C_3}\right)A\right]\right\}$$
$$= \frac{\omega_1^2}{pq+\omega_1^2}\left\{\frac{B_1}{B_3} + \frac{C_1}{C_3} + \left[\frac{B_1}{B_3}\left(\frac{B_2}{B_1}-\frac{B_4}{B_3}\right) + \frac{C_1}{C_3}\left(\frac{C_2}{C_1}-\frac{C_4}{C_3}\right)\right]A\right\}$$
$$= \Delta\omega^2\frac{A}{\chi+A}(D_1+D_2A), \quad (A.5)$$

where $\chi = \frac{pq}{\Delta\omega^2}$, $D_1 = \frac{B_1}{B_3} + \frac{C_1}{C_3}$, and $D_2 = \frac{B_1}{B_3}\left(\frac{B_2}{B_1}-\frac{B_4}{B_3}\right) + \frac{C_1}{C_3}\left(\frac{C_2}{C_1}-\frac{C_4}{C_3}\right)$. By solving $\frac{\partial(\mathrm{PTR})}{\partial A} = 0$, the optimal RF power can be written as:

$$\omega_1 = \Delta\omega\sqrt{\sqrt{\chi^2 - \frac{D_1}{D_2}\chi} - \chi}. \quad (A.6)$$

References

[1] H.M. McConnell, Reaction rates by nuclear magnetic resonance, J. Chem. Phys. 28 (1958) 430–431.

[2] D.E. Woessner, Nuclear transfer effects in nuclear magnetic resonance pulse experiments, J. Chem. Phys. 35 (1961) 41–48.

[3] S. Forsen, R.A. Hoffman, Study of moderately rapid chemical exchange reactions by means of nuclear magnetic double resonance, J. Chem. Phys. 39 (1963) 2892–2901.

[4] A. Allerhand, H.S. Gutowsky, Spin–echo NMR studies of chemical exchange. I. Some general aspects, J. Chem. Phys. 41 (1964) 2115–2126.

[5] J. Jeener, B.H. Meier, P. Bachmann, R.R. Ernst, Investigation of exchange processes by two-dimensional NMR spectroscopy, J. Chem. Phys. 71 (1979) 4546–4553.

[6] J. Schotland, J.S. Leigh, Exact solutions of the Bloch equations with *n*-site chemical exchange, J. Magn. Reson. 51 (1983) 48–55.

[7] S.D. Wolff, R.S. Balaban, NMR imaging of labile proton exchange, J. Magn. Reson. 86 (1990) 164–169.

[8] V. Guivel-Scharen, T. Sinnwell, S.D. Wolff, R.S. Balaban, Detection of proton chemical exchange between metabolites and water in biological tissues, J. Magn. Reson. 133 (1998) 36–45.

[9] K.M. Ward, A.H. Aletras, R.S. Balaban, A new class of contrast agents for MRI based on proton chemical exchange dependent saturation transfer (CEST), J. Magn. Reson. 143 (2000) 79–87.

[10] N. Goffeney, J.W.M. Bulte, J. Duyn, L.H. Bryant, P.C.M. van Zijl, Sensitive NMR detection of cationic-polymer-based gene delivery systems using saturation transfer via proton exchange, J. Am. Chem. Soc. 123 (2001) 8628–8629.

[11] S. Zhang, P. Winter, K. Wu, A.D. Sherry, A novel europium(III)-based MRI contrast agent, J. Am. Chem. Soc. 123 (2001) 1517–1578.

[12] S. Aime, A. Barge, D. Delli Castelli, F. Fedeli, A. Mortillaro, F.U. Nielsen, E. Terreno, Paramagnetic Lanthanide(III) complexes as pH-sensitive chemical exchange saturation transfer (CEST) contrast agents for MRI applications, Magn. Reson. Med. 47 (2002) 639–648.

[13] S. Zhang, M. Merritt, D.E. Woessner, R. Lenkinski, A.D. Sherry, PARACEST agents: modulating MRI contrast via water proton exchange, Acc. Chem. Res. 36 (2003) 783–790.

[14] J. Zhou, J. Payen, D.A. Wilson, R.J. Traystman, P.C.M. van Zijl, Using the amide proton signals of intracellular proteins and peptides to detect pH effects in MRI, Nature Med. 9 (2003) 1085–1090.

[15] J. Zhou, B. Lal, D.A. Wilson, J. Laterra, P.C.M. van Zijl, Amide proton transfer (APT) contrast for imaging of brain tumors, Magn. Reson. Med. 50 (2003) 1120–1126.

[16] R.G.S. Spencer, A. Horska, J.A. Ferretti, G.H. Weiss, Spillover and incomplete saturation in kinetic measurements, J. Magn. Reson. B 101 (1993) 294–296.

[17] A. Horska, R.G.S. Spencer, Correctly accounting for radiofrequency spillover in saturation transfer experiments: application to measurement of the creatine kinase reaction rate in human forearm muscle, MAGMA 5 (1997) 159–163.

[18] E. Baguet, C. Roby, Off-resonance irradiation effect in steady-state NMR saturation transfer, J. Magn. Reson. 128 (1997) 149–160.

[19] P.B. Kingsley, W.G. Monahan, Effects of off-resonance irradiation, cross-relaxation, and chemical exchange on steady-state magnetization and effective spin–lattice relaxation times, J. Magn. Reson. 143 (2000) 360–375.

[20] P.B. Kingsley, W.G. Monahan, Correction for off-resonance effects and incomplete saturation in conventional (two-site) saturation-transfer kinetic measurements, Magn. Reson. Med. 43 (2000) 810–819.

[21] E. Baguet, C. Roby, Fast inversion-recovery measurements in the presence of a saturating field for a two-spin system in chemical exchange, J. Magn. Reson. A 108 (1994) 189–195.

[22] J. Zhou, D.A. Wilson, P.Z. Sun, J.A. Klaus, P.C.M. van Zijl, Quantitative description of proton exchange processes between water and endogenous and exogenous agents for WEX, CEST, and APT experiments, Magn. Reson. Med. 51 (2004) 945–952.

[23] R.S. Balaban, T.L. Ceckler, Magnetization transfer contrast in magnetic resonance imaging, Magn. Reson. Q. 8 (1992) 116–137.

[24] R.M. Henkelman, G.J. Stanisz, S.J. Graham, Magnetization transfer in MRI: a review, NMR Biomed. 14 (2001) 57–64.

[25] R.M. Henkelman, X. Huang, Q.-S. Xiang, G.J. Stanisz, S.D. Swanson, M.J. Bronskill, Quantitative interpretation of magnetization transfer, Magn. Reson. Med. 1993 (1993) 759–766.

[26] G. Helms, G.E. Hagberg, Pulsed saturation of the standard two-pool model for magnetization transfer. Part I: the steady state, Concepts Magn. Reson. A 21 (2004) 37–49.
[27] X. Wu, J.J. Listinsky, Effects of transverse cross relaxation on magnetization transfer, J. Magn. Reson. B 105 (1994) 73–76.
[28] R.G. Bryant, The dynamics of water-protein interactions, Annu. Rev. Biophys. Biomol. Struct. 25 (1996) 29–53.
[29] J.M. Hakumaki, O.H. Grohn, T.R.M. Pirttila, R.A. Kauppinen, Increased macromolecular resonances in the rat cerebral cortex during severe energy failure as detected by ^{1}H nuclear magnetic resonance spectroscopy, Neurosci. Lett. 212 (1996) 151–154.